

**Original articles**

Research article

<https://doi.org/10.17308/kcmf.2024.26/12043>**Theoretical exploration of halogenated anthracene derivatives: unraveling electronic and molecular insights****K. A. Othman¹✉, Y. H. Azeez², R. A. Omer^{1,3}, R. O. Kareem²**¹*Koya University, Faculty of Science & Health, Department of Chemistry, Koya KOY45, Kurdistan Region – F.R., Iraq*²*University of Halabja, College of Science, Department of Physics, Halabja 46018, Iraq*³*Department of Pharmacy, College of Pharmacy, Knowledge University, Erbil 44001, Iraq***Abstract**

This research article delves into the profound ramifications of halogenation on anthracene within the captivating domain of polycyclic aromatic hydrocarbons (PAHs). By employing Density Functional Theory (DFT) calculations, the study comprehensively explores the intricate interplay between halogen atoms and the molecular framework of anthracene. The entwining of halogens such as fluorine, chlorine, and bromine with aromatic rings orchestrates a symphony of changes, reshaping electronic structures, reactivity, and optical behaviors. This investigation traverses diverse analytical landscapes, encompassing molecular orbitals and Density of States analysis, UV-visibility spectra, infrared spectroscopy, nuclear magnetic resonance (NMR), and natural bond orbital (NBO) analysis, unveiling the intricate tapestry of molecular modifications. The electronic transitions, vibrational signatures, and NMR shifts of halogenated derivatives illuminate the dynamic effects of halogenation. Moreover, the study contemplates their potential across medicinal, environmental, and optoelectronic landscapes. Ultimately, this exploration presents a comprehensive narrative that harmonizes theoretical insights with practical applications.

Keywords: PAHs, Halogenation, Electronic Properties, DFT, Energy States, Frequency Analysis**Acknowledgments:** We would like to thank the heads of the chemistry departments at Koya University for their support.**For citation:** Othman K. A., Azeez Y. H., Omer R. A., Kareem R. O. Theoretical exploration of halogenated anthracene derivatives: unraveling electronic and molecular insights. *Condensed Matter and Interphases*. 2024;26(2): 280–294. <https://doi.org/10.17308/kcmf.2024.26/12043>**Для цитирования:** Осман Х. А., Азиз Ю. Х., Омер Р. А., Карим Р. О. Теоретическое исследование галогенированных производных антрацена: электронный и молекулярный аспект. *Конденсированные среды и межфазные границы*. 2024;26(2): 280–294. <https://doi.org/10.17308/kcmf.2024.26/12043>✉ Khdir A. Othman, khdir.ahmed@koyauniversity.org

© Othman K. A., Azeez Y. H., Omer R. A., Kareem R. O., 2024



The content is available under Creative Commons Attribution 4.0 License.

1. Introduction

Anthracene, a fundamental polycyclic aromatic hydrocarbon (PAH), embodies the intricate interplay among fused aromatic rings [1, 2]. Recent scientific attention has pivoted towards understanding the transformative impact of halogenation on these molecules, with halogens like fluorine, chlorine, and bromine intricately engaging with anthracene and reshaping its potential [3]. Halogenation is a precision tool that crafts a fresh narrative for PAHs, meticulously refining electronic structure and reactivity, altering energy levels, influencing absorption spectra, and sculpting fluorescence behavior [4–6]. The derivatives of halogenated anthracene beckon across diverse scientific horizons. In the realm of medicine, these derivatives hold promise as antibacterial and antifungal agents, candidates for innovative therapies against cancer and infectious diseases, and as components of advanced drug delivery systems [7–11]. Environmental considerations arise as halogenated PAHs traverse the realms of air, water, and soil, shaping their destiny and toxicity profiles, underscoring the importance of ecological understanding [12–14].

In this research endeavor, we embark on a computational journey, dissecting the effects of halogenation on anthracene and its derivatives. Employing analytical methods spanning molecular orbitals, UV-visibility, IR spectroscopy, NMR, Potential Energy Maps (PES), and more, we unravel the intricate tapestry of these molecules. From unraveling drug likeness to unveiling electronic intricacies, this study contributes to comprehending halogenated anthracene derivatives and their applications.

2. Computational procedure

In this study, Density Functional Theory (DFT) calculations were conducted using the Gaussian 09 computational package. The B3LYP functional was employed for molecular optimization, employing the 6-311G basis set [15–18].

3. Results and discussion

Anthracene and its derivatives doped with fluorine, chlorine, and bromine underwent design via GaussView. Subsequently, a DFT model was employed to optimize their structures,

utilizing the B3LYP/6-311G basis set known for its appropriateness in capturing low-energy configurations (i.e., basis set with the lowest energy [19–21]).

3.1. Molecular orbitals (MOs) and density of states (DOS) analysis

MOs and DOS analysis are pivotal for comprehending a material's electronic structure [22–24]. MOs define electron distribution within molecules, while DOS analysis illustrates energy level distribution (Figs. 1, 2). The energy gap, exemplified by the difference between the Highest Occupied Molecular Orbital (HOMO) and Lowest Unoccupied Molecular Orbital (LUMO) energies, significantly influences reactivity and optical attributes [25, 26]. For instance, in the context of halogen-doped anthracene, the undoped molecule displays a HOMO-LUMO gap of 3.5785 eV. Upon fluorine, chlorine, or bromine substitution, this gap decreases by 0.0069, 0.0224, and 0.0301 eV respectively, due to changes in electron distribution. This interplay between MOs, DOS analysis, and energy gap values offers a comprehensive understanding of electronic transitions, reactivity, and optical behavior in the realm of molecules and materials [27, 28]. Fig. 2 shows that the halogen-doped structures have higher DOS than anthracene, which means they have more available electron states at a given energy level. This could affect their electrical and optical properties.

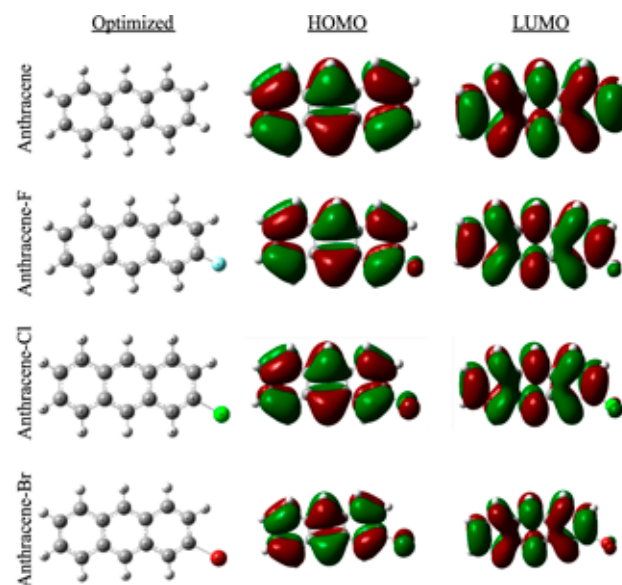


Fig. 1. Optimized structures and MOs of anthracene and its structures doped with halogens

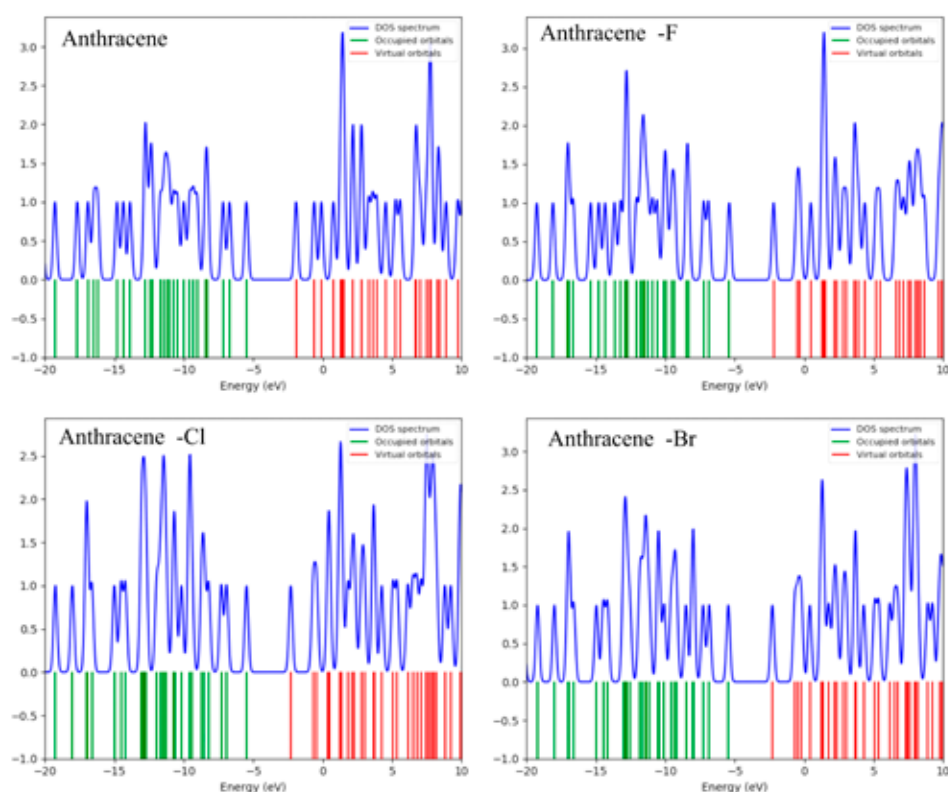


Fig. 2. DOS analysis for anthracene and its halogen-doped structures

The quantum chemical parameters of anthracene and its halogen-substituted derivatives vary systematically with the size of the halogen atom (Table 1). For example, the total energy of the compounds decreases as the halogen atom becomes larger [29], from -14684.7709 eV for anthracene to -84714.4531 eV for anthracene-Br. This is because the halogen atoms have more electrons, Doping anthracene with halogens leads to a decrease in E_{HOMO} and E_{LUMO} . This effect is due to the higher electronegativity of halogen atoms, causing electron repulsion from the aromatic ring. Consequently, the ΔE (HOMO-LUMO gap) of the compounds decreases in the order anthracene > anthracene-F > anthracene-Cl > anthracene-Br, indicating increased polarizability with larger halogen atoms [30–32].

The ionization potential (I) and electron affinity (A) of anthracene and its halogen derivatives increase with the size of the halogen atom, from 5.4899 eV and 1.9114 eV for anthracene to 5.6988 eV and 2.1504 eV for anthracene-Br, respectively. This is due to the lower HOMO and LUMO energies, which affect the ease of electron removal and addition [33]. The chemical hardness (η) and softness (S) of anthracene and

its halogen derivatives are inversely related to the size of the halogen atom [34]. The η values decrease from 1.7892 eV for anthracene to 1.7742 eV for anthracene-Br, due to the smaller HOMO-LUMO gap and higher polarizability. The S values increase from 0.5589 eV $^{-1}$ for anthracene to 0.5636 eV $^{-1}$ for anthracene-Br, due to the smaller HOMO-LUMO gap and higher reactivity. The electrophilicity (ω) and nucleophilicity (Nu) of anthracene and its derivatives vary with the halogen doping. The ω values exhibit an ascending trend from 3.8269 eV for anthracene to 4.3407 eV for anthracene-Br, due to the enhanced electrophilic nature of the halogens. The Nu values display a descending trend accordingly [35, 36]. The different halogen substituents (F, Cl, Br) have an impact on the electronic properties of the compounds, influencing parameters like ΔE backdonation and the transfer electron fraction ΔN (Fe). The specific effects are influenced by the nature of the halogen atom and its electronic interactions within the molecular structure

3.2. Ultraviolet-visible (UV-Vis) analysis

Gaussian software facilitated energy calculations, optimizing the structure with the

6-311G(d,p) basis set. The TD-SCF method was applied for electronic transition and absorption spectrum analysis [37–39]. Fig. 3 illustrates absorption coefficient variation with incident light wavelength, highlighting greater coefficients representing enhanced light absorption.

Anthracene possesses a series of conjugated double bonds, which impart it with various intriguing properties, notably its capability to absorb UV light [40–42].

Anthracene doping with the first three halogens increases electron density in the HOMO and LUMO orbitals. This reduces the energy gap between the HOMO and LUMO orbitals and affects the optical properties of the anthracene molecule. Consequently, the electrons at the HOMO of the doped molecules require energy with a lower frequency and higher wavelength to transition from HOMO to LUMO [43]. This phenomenon enhances the likelihood of the doped molecules absorbing light in the visible spectrum (Fig. 3). As a result, the doped molecules exhibit more pronounced coloration compared to the undoped molecules (i.e., $\lambda = 382.8, 384.3, 387,$ and 430.2 nm for Anthracene,

anthracene-F, anthracene-Br, and anthracene-Cl respectively).

3.3. Infrared (IR) analysis

Gaussian software was utilized to perform energy calculations, resulting in the optimized structure obtained through the 6-311G(d,p) basis set [40, 44].

The identification of conjugated rings within the anthracene structure is facilitated by its distinctive aromatic C–H stretching. Notably, the C–H stretching vibrations of PAHs are commonly observed around 3100 cm^{-1} [45–49]. This study calculates the theoretically estimated aromatic C–H stretching vibrational modes within the range of $3154\text{--}3188\text{ cm}^{-1}$ (Fig. 4).

The study's exploration of halogen doping's impact on the infrared (IR) spectra of anthracene uncovers noteworthy transformations. Initially, the introduction of halogen atoms induces shifts in absorption peak positions, signifying changes in molecular vibrations and bond strengths (e.g., C=C-H in undoped anthracene at $3154\text{--}3188\text{ cm}^{-1}$, shifting to $3295\text{--}3321\text{ cm}^{-1}$ for fluorine-doped anthracene). Moreover, novel absorption bands

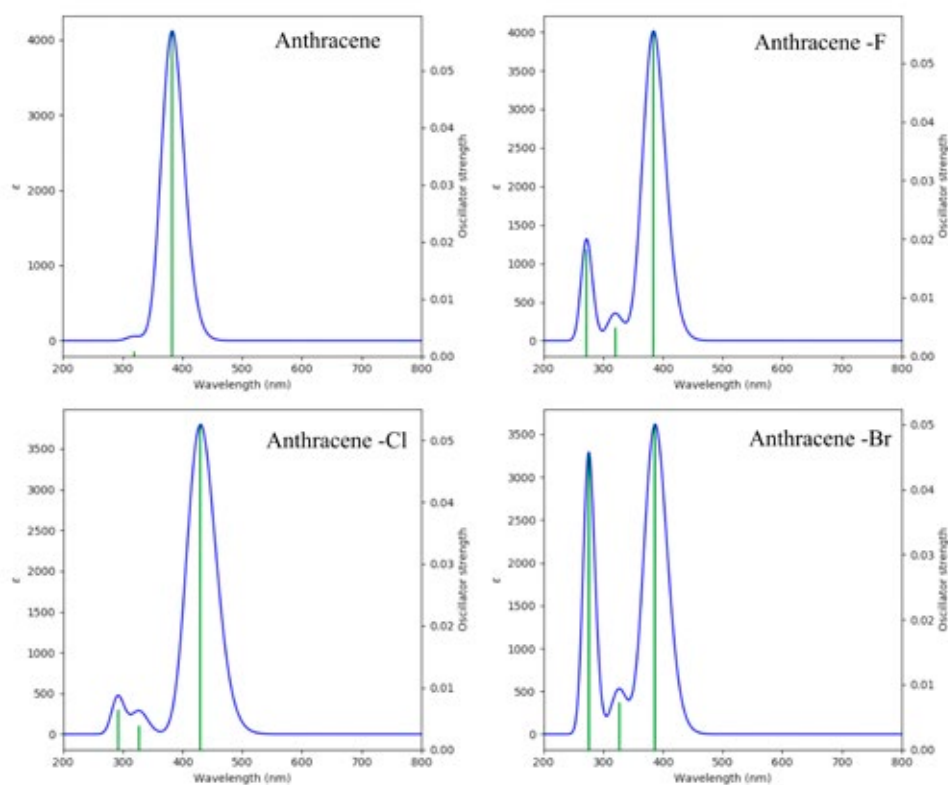


Fig. 3. UV-Vis. absorption spectra of anthracene and its halogen-doped derivatives

emerge, indicating the formation of fresh vibrational modes and functional groups. The study also detects alterations in intensity and band width for specific absorption peaks, indicative of variations in molecular flexibility and rigidity. Notably, the presence of halogen atoms introduces distinct IR absorption peaks linked to the halogen groups themselves. Collectively, this investigation offers valuable insights into the modifications induced by halogen doping, shedding light on their intricate influence on the IR spectra of these molecules.

3.4. Nuclear magnetic resonance (NMR)

Fig. 5 illustrates the theoretically computed H-NMR and C-NMR structures for both pristine anthracene and its derivatives doped with the first three halogen group members. The NMR calculations were performed using Gaussian 09 software. The shielding range for normal anthracene spans from -50 to 100 ppm [24]. Notably, introducing fluorine caused a ppm shift ranging from -100 to 300 ppm. This ppm shifts persisted when chlorine replaced fluorine, spanning from -200 to 700 ppm. With

the introduction of bromine, the ppm shift intensified, ranging from -500 to 2000 ppm. This trend indicated an expanded shielding range corresponding to the increasing electronegativity of the halogen family. Fig. 5 portrays the original NMR peaks of undoped anthracene, with more carbon resonances at the upfield and fewer at the downfield. The introduction of fluorine led to a notable transformation in molecule orientation. A distinct medium peak for fluorine emerged at 290.128 ppm, while carbon and hydrogen atoms underwent chemical environment changes due to inductive and neighboring effects. The same pattern held when chlorine and later bromine replaced fluorine, manifesting peaks at 704.749 and 1968.174 ppm, respectively. This observation underscores the linear relationship between NMR peaks generated by halogen family members in anthracene and their electronegativity.

3.5. Potential energy map (PEM) and charge distribution

The PES and charge distribution significantly impact the molecular orientation and influence the optical and electrical properties of the

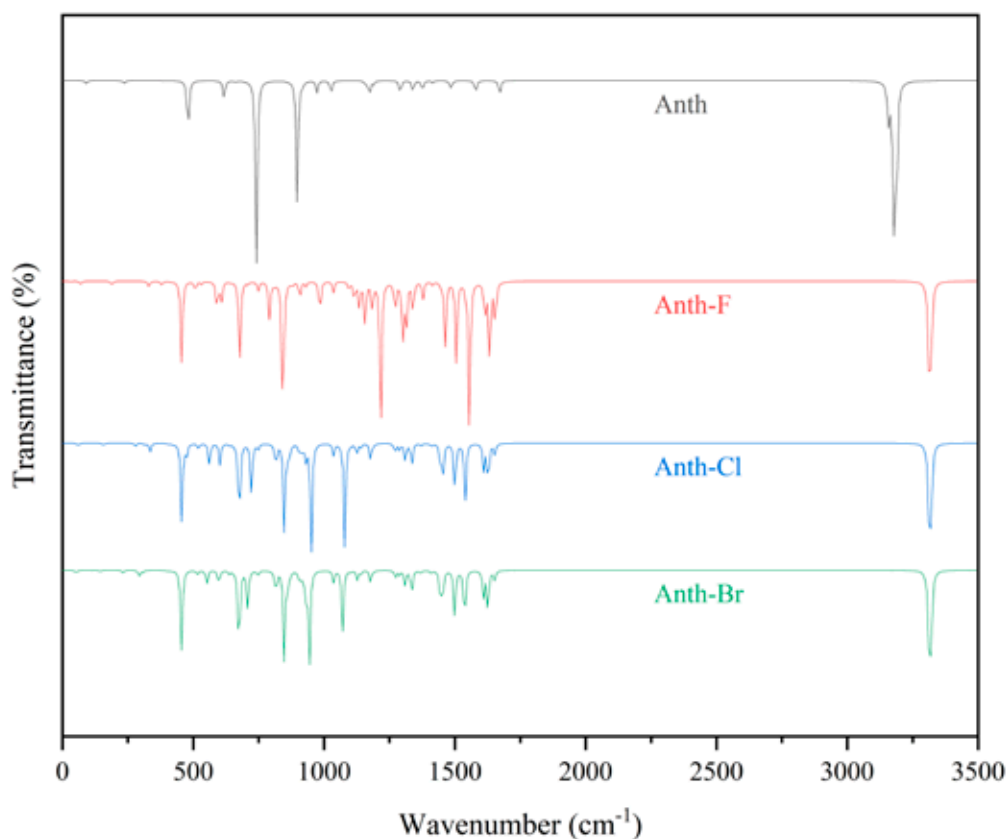


Fig. 4. IR spectrum for anthracene and its halogenation with F, Cl and Br

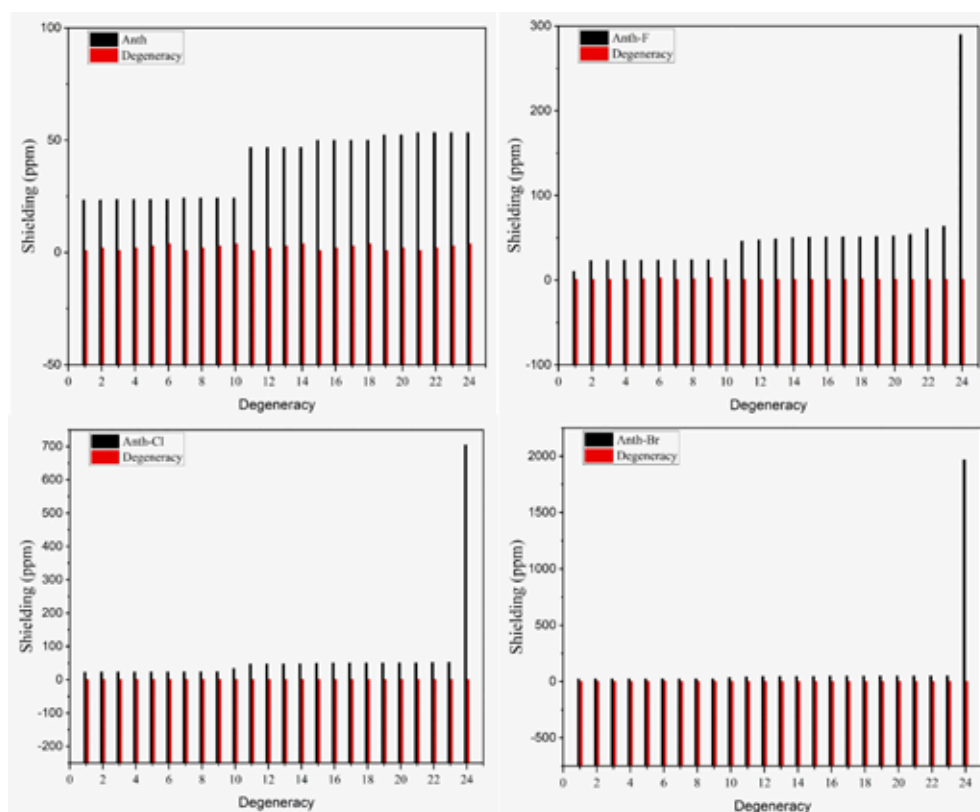


Fig. 5. NMR of anthracene and its halogen-doped derivatives

molecules [50–52]. Fig. 6 shows the PESs of anthracene and its halogen-doped derivatives. These maps illustrate how the charge distribution of a molecule varies in three dimensions, using different colors to indicate high and low charge density regions. The charge distribution is calculated as the net charge on each atom or group of atoms in a molecule. The arrows in Figure 6 represent the direction and magnitude of the dipole moments of each molecule. The dipole moment is a vector quantity that measures the molecular polarity, or the degree of separation

of positive and negative charges in a molecule. A higher dipole moment indicates a more polar molecule.

Anthracene has a symmetrical charge distribution and no net dipole moment, as shown in Fig. 6 and Table 1. This means that it is a non-polar molecule with no net charge. However, when anthracene is doped with halogens, such as fluorine, chlorine, or bromine, its charge distribution and polarity change dramatically. Halogens are more electronegative than carbon and hydrogen [53], which means that they pull

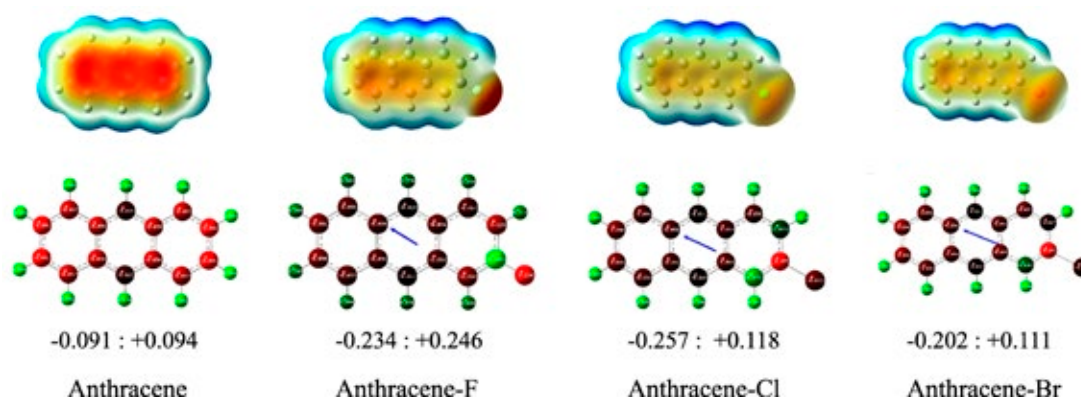


Fig. 6. PEM and charge distributions for anthracene and its halogen-doped structures

Table 1. Quantum chemical parameter's values of study compounds

Quantum chemical parameters	Anthanthrene	Anthanthrene-F	Anthanthrene-Cl	Anthanthrene-Br
Total Energy (eV)	-14684.7709	-17385.8899	-27191,7283	-84714.4531
E_{HOMO} (eV)	-5.4899	-5.6231	-5.7072	-5.6988
E_{LUMO} (eV)	-1.9114	-2.0515	-2.1511	-2.1504
ΔE (eV)	3.5785	3.5716	3.5561	3.5484
Ionization potential I (eV)	5.4899	5.6231	5.7072	5.6988
Electron affinity A (eV)	1.9114	2.0515	2.1511	2.1504
Chemical hardness « η » (eV)	1.7892	1.7858	1.7780	1.7742
Chemical softness S (eV ⁻¹)	0.5589	0.5600	0.5624	0.5636
Electronegativity χ (eV)	3.7006	3.8373	3.9292	3.9246
Chemical potential μ (eV)	-3.7006	-3.8373	-3.9292	-3.9246
Electrophilicity ω (eV)	3.8269	4.1228	4.3414	4.3407
Nucleophilicity Nu (eV ⁻¹)	0.2613	0.2426	0.2303	0.2304
ΔE backdonation	-0.4473	-0.4464	-0.4445	-0.4436
Transfer electron fraction ΔN	2.9517	2.8239	2.7300	2.7282
Dipole-moment (Debye), « μD »	0.0000	1.7247	2.3449	2.2182

more electrons towards themselves. This causes a shift of electron density from the carbon rings to the halogen atom, creating an asymmetrical charge distribution and a net dipole moment in the molecule. Table 1 show that chlorine-doped anthracene has the largest dipole moment (2.3449), followed by bromine-doped (2.2182), and fluorine-doped anthracene (1.7247). This implies that chlorine-doped anthracene is the most polar and reactive molecule among the four shown in Fig. 6.

3.6. Reduced density gradient (RDG) and noncovalent interactions (NCI)

The innovative utilization of reduced density gradient (RDG) and noncovalent interactions (NCI) has revolutionized the exploration of weak intermolecular forces. Through the RDG methodology, the NCI index serves as a compelling tool to substantiate non-covalent interactions. RDG is a dimensionless parameter that synergizes density and its derivative. Employing Multiwfn for RDG in eq. (1) scatter plots and VMD for 3D isosurfaces, the visualization of these intricate interactions is enriched:

$$RDG(r) = \frac{1|\nabla\rho(r)|}{2(3\pi r^2)^{\frac{1}{3}}\rho^{\frac{4}{3}}(r)}. \quad (1)$$

The investigative NCI pursuits are founded on an isosurface threshold of 0.5, within the

RDG isosurface scope of -0.035 to 0.02 atomic units, as elegantly showcased in Fig. 7. This analysis is further elevated through graphical representation, which correlates the function $\rho(r)$ with the sign of λ_2 , offering profound insights into molecular interactions. The polarity of $\text{sign}(\lambda_2)\rho$ yields invaluable predictions: a negative value signifies attractive, bound interactions, while a positive value signifies repulsive, non-bonded interactions. The scatter graphs in Fig. 7 transcends visual complexity. By stratifying spikes based on $\text{sign}(\lambda_2)\rho$, distinct color-coded zones emerge—red for robust repulsion, green for delicate attraction (van der Waals), and blue for potent intermolecular interactions, particularly robust hydrogen bonding. These advancements underscore the pivotal role of RDG and NCI methodologies in decoding intricate intermolecular dynamics [54–58].

When compared to other compounds, those containing fluorine display a heightened concentration of points on the graph. This finding indicates that weak hydrogen bonds and van der Waals interactions within fluorine-containing compounds are more robust. This insight is underscored by the red patches in Fig. 7, which are localized within aromatic rings and signify significant repulsive interactions. Furthermore, in the same Fig. 7, a green isosurface linked to the anthracene compound emerges, highlighting van der Waals interactions. This specific isosurface's

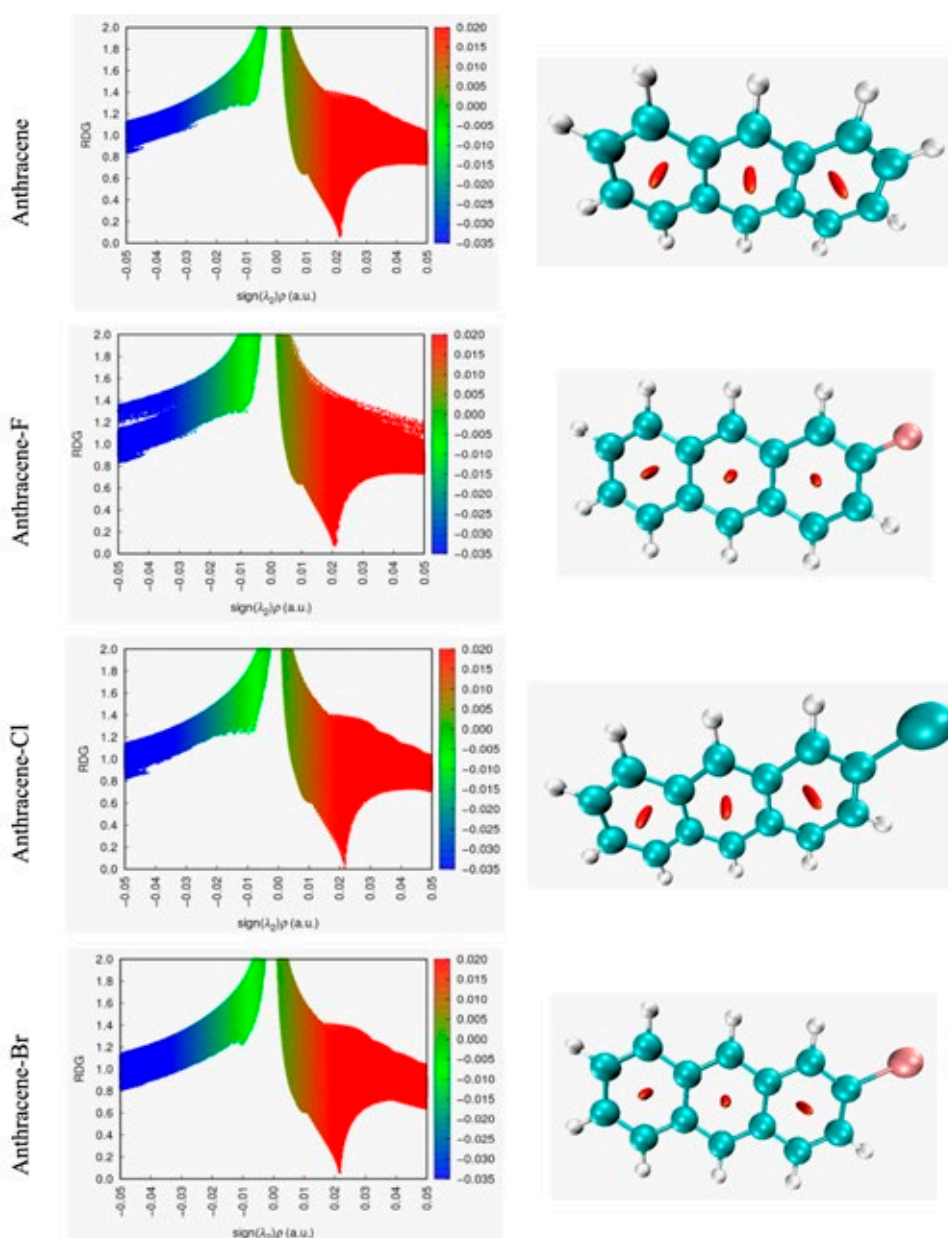


Fig. 7. RDG Analysis of Studied Compounds – Weak and Strong Interactions

positioning corroborates the presence of these interactions. Simultaneously, it provides evidence for weak hydrogen bonding and additional hydrogen-hydrogen contacts (H–H).

Evaluating a compound's potential as a drug involves essential steps, often employing Molinspiration property values in alignment with Lipinski's rule of five. This widely recognized guideline suggests that successful drugs typically adhere to specific criteria: fewer than five hydrogen bond donors, less than ten hydrogen bond acceptors, a molar refractivity within 40 to 160, a polar surface area below 140 \AA^2 , a molecular

weight under 500, and containing fewer than ten rotatable bonds [59, 60].

Table 2 shows how the molecular properties of anthracene and its halogenated derivatives vary depending on the type of halogen attached. The molecular weight of anthracene increases with the size and polarizability of the halogen, making it less volatile and dense. The HBA of anthracene increases by one when fluorine is added, enhancing its hydrogen bonding and solubility. The PSA of anthracene and its derivatives remains zero, indicating a low polarity and a high permeability. These properties

Table 2. Molinspiration property values for the studied compounds

Descriptors	Anthracene				Expected range
	Neutral	+Cl	+Br	+F	
Hydrogen bond donor (HBD)	0	0	0	0	5
Hydrogen bond acceptors (HBA)	0	0	0	1	10
Molar Refractivity	61.45	66.46	69.15	61.41	40–160
Polar surface area (PSA) Å ²	0.00	0.00	0	0	140
Molecular weight	178.23	212.67	257.13	196.22	500
Number of rotatable bonds	0	0	0	0	10

are important for the chemical and biological behavior of these molecules.

3.7. Natural bond orbital (NBO) analysis

Utilizing B3LYP/6–31G(d, p) theoretical methods, this study extensively investigated the NBO configuration of the compound in question. The main focus was on elucidating interactions between Lewis and non-Lewis orbitals, shedding light on intramolecular and intermolecular hydrogen bonding, as well as π electron dispersion. Stabilization energy, a measure of delocalization interactions, was evaluated using second-order energy for individual donor NBOs (i) and acceptor NBOs (j) in eq. (2), leading to $E^{(2)}$ values capturing electron delocalization. This concept is mathematically expressed by the equation [61–65]:

$$E^{(2)}q = \Delta E_{ij} = q_i \frac{F(i, j)^2}{\epsilon_j - \epsilon_i} \quad (2)$$

Here, “ q_i ” denotes donor orbital occupancy, “ ϵ_j ” and “ ϵ_i ” represent diagonal elements, and “ $F(i, j)$ ” signifies NBO Fock matrix elements. Table 3 provides an in-depth exploration through Second Order Perturbation Theory Analysis of the Fock Matrix in NBO for a range of compounds, specifically Anthracene and its derivatives: Anthracene (neutral), Anthracene (+Cl), Anthracene (+Br), and Anthracene (+F). The table unveils a rich tapestry of insights into the interactions between donor and acceptor NBOs, revealing $E^{(2)}$ values that correspond to significant stabilization energies. Moreover, it showcases the differences in energy ($E(j) - E(i)$) in atomic units and the associated $F(i, j)$ values in atomic units, further underlining the complex interplay of

forces within these molecules. Drawing attention to specific examples, Anthracene (+Br) stands out with a remarkable transition, as the LP (3) Br 24 orbital donates to the π^* C 17 – C 20 acceptor, resulting in a substantial stabilization energy of 78.61 kcal/mol. This transition underscores the magnitude of intermolecular interactions, indicative of a strong binding affinity between the Br atom and the phenyl ring. Comparing across the various derivatives, Anthracene (+F) demonstrates noteworthy interactions as well. Here, π C 1 – C 6 engages with π^* C 4 – C 5, leading to a stabilization energy of 17.39 kcal/mol. This interaction, while energetically favorable, highlights the relatively weaker influence of fluorine compared to other substituents like chlorine and bromine.

3.8. Nonlinear optical (NLO) properties

NLO materials are of paramount importance in the realm of nonlinear optics, playing a pivotal role in fields such as information technology and various industrial applications. The optimization of geometry was carried out through the B3LYP/6-31G+(d,p) method, followed by an initial static analysis. The computation of the three-dimensional tensor, denoted as (β_0) representing the initial static hyperpolarizability, involved equations for its x, y, and z components (eq. (3)). These components contribute to determining the overall static dipole moment (μ_t), the mean polarizability (α_0), and the initial static hyperpolarizability (β_0) [61, 66]:

$$\mu_t = \left[\mu_x^2 + \mu_y^2 + \mu_z^2 \right]^{1/2},$$

$$\alpha_t = \frac{(\alpha_{xx} + \alpha_{yy} + \alpha_{zz})}{3},$$

Table 3. Second order perturbation theory analysis of Fock Matrix in NBO for Studied Compounds

Anthracene (neutral)				
Donor NBO (<i>i</i>)	Acceptor NBO (<i>j</i>)	<i>E</i> (2) kcal/mol	<i>E</i> (<i>j</i>)– <i>E</i> (<i>i</i>) a.u.	<i>F</i> (<i>i,j</i>) a.u.
π C 1 – C 2	π^* C 3 – C 4	17.63	0.28	0.063
π C 1 – C 2	π^* C 9 – C 10	18.4	0.29	0.068
σ C 1 – H 7	σ^* C 5 – C 6	4.96	1.04	0.064
π C 9 – C 10	π^* C 1 – C 2	17.17	0.3	0.066
π C 9 – C 10	π^* C 11 – C 12	16.43	0.3	0.063
σ C 9 – H 13	σ C 2 – C 3	4.59	1.04	0.062
π C 18 – C 19	LP (1) C 5	35.32	0.16	0.085
LP (1) C 5	π^* C 3 – C 4	69.28	0.14	0.106
LP (1) C 5	π^* C 18 – C 19	52.46	0.14	0.099
LP*(1) C 6	π^* C 1 – C 2	69.27	0.14	0.106
Anthracene (+Cl)				
π C 1 – C 2	π^* C 9 – C 10	21.32	0.28	0.071
σ C 1 – H 7	σ^* C 5 – C 6	4.65	1.1	0.064
σ C 2 – C 9	σ^* C 2 – C 3	4.76	1.26	0.069
σ C 6 – C 17	σ^* C 20 – Cl 24	5.09	0.83	0.058
π C 11 – C 12	π^* C 9 – C 10	19.14	0.28	0.066
π C 18 – C 19	π^* C 4 – C 5	18.92	0.29	0.069
LP*(1) C 3	π^* C 1 – C 2	72.87	0.14	0.107
LP (1) C 6	π^* C 1 – C 2	67.29	0.14	0.104
LP (1) C 6	π^* C 17 – C 20	78.61	0.12	0.106
π^* C 17 – C 20	π^* C 18 – C 19	191.31	0.01	0.077
Anthracene (+Br)				
σ C 1 – C 6	σ^* C 5 – C 6	4.85	1.26	0.07
σ C 6 – C 17	σ^* C 20 – Br 24	5.23	0.78	0.057
π C 9 – C 10	π^* C 1 – C 2	19.86	0.29	0.07
π C 11 – C 12	π^* C 9 – C 10	19.13	0.28	0.066
σ C 12 – H 16	σ^* C 2 – C 3	4.85	1.1	0.066
σ C 18 – C 19	σ^* C 20 – Br 24	5.32	0.79	0.058
LP*(1) C 3	π^* C 1 – C 2	72.77	0.14	0.107
LP (1) C 6	π^* C 17 – C 20	78.4	0.12	0.106
LP (3) Br 24	π^* C 17 – C 20	10.54	0.31	0.054
π^* C 17 – C 20	π^* C 18 – C 19	196.36	0.01	0.077
Anthracene (+F)				
π C 1 – C 6	π^* C 4 – C 5	17.39	0.28	0.063
π C 1 – C 6	π^* C 17 – C 20	18.45	0.28	0.066
σ C 1 – H 7	σ^* C 2 – C 3	4.97	1.04	0.064
σ C 4 – H 8	σ^* C 5 – C 6	5.01	1.04	0.065
π C 17 – C 20	π^* C 18 – C 19	15.31	0.31	0.062
π C 18 – C 19	π^* C 4 – C 5	15.86	0.3	0.065
LP*(1) C 2	π^* C 1 – C 6	69.7	0.14	0.105
LP*(1) C 2	π^* C 9 – C 10	51.66	0.14	0.098
LP (1) C 3	π^* C 11 – C 12	52.31	0.14	0.099
LP (3) F 24	π^* C 17 – C 20	19.73	0.44	0.087

$$\beta_t = (\beta_x^2 + \beta_y^2 + \beta_z^2)^{\frac{1}{2}} \beta_x = \beta_{xxx} + \beta_{xyz} + \beta_{xzz} \beta_y = \beta_{yy} + (3) \\ + \beta_{xy} + \beta_{yz} \beta_z = \beta_{zzz} + \beta_{xxz} + \beta_{yzz}.$$

Notably, significant magnitudes of specific polarizability and hyperpolarizability components indicate a pronounced dispersion of charge in particular orientations [67, 68] Table 4 presents the computed values for compounds with different substitutions (+Cl, +Br, +F), revealing their molecular dipole moments (μ), mean polarizabilities (α_0), and initial hyperpolarizabilities (β_0). These values, initially provided in atomic units (a.u.), have been conveniently converted into electrostatic units (e.s.u.) for better comparability. Remarkably, the dipole moments of the compounds (+Cl, +Br, +F) surpass that of the well-known molecule Urea ($\mu = 1.3732$ D), often employed as a benchmark in NLO investigations.

Turning to polarizabilities, the results highlight that anthracene exhibits heightened polarizability when subjected to a positive inductive effect (+F), whereas Anthracene displays reduced polarizability under a positive inductive effect (+Br). In the context of NLO systems, the magnitude of (β_0) holds substantial significance. Notably, the computed β_0 values for the examined compounds are comparatively lower than the benchmark value of urea ($343.272 \cdot 10^{-33}$ esu), suggesting that these compounds might have limited potential for practical NLO applications.

4. Conclusions

In this comprehensive research article, the profound impact of halogenation on anthracene has been intricately unveiled. Through DFT calculations, we navigated the intricacies of electronic structure, reactivity, and optical behavior as they respond to the presence of halogen atoms. The resulting insights underscore the delicate symphony of changes introduced by halogens like fluorine, chlorine, and bromine, reshaping the properties and potential of these PAHs. Analytical explorations, spanning MOs, UV-visibility spectra, vibrational signatures, NMR shifts, and NBO analysis, collectively illustrate the multifaceted impact of halogenation. This research extends beyond theoretical boundaries to embrace practical realms, offering glimpses

Table 4. Nonlinear optical properties of the title compounds

Parameters	Anthracene			
	Neutral	+Cl	+Br	+F
μ_x	0.00	1.00	-0.91	0.16
μ_y	0.00	2.11	1.96	1.72
μ_z	0.00	0.00	0.00	0.00
μ_t	0.00	2.33	2.16	1.73
α_{xx}	-88.00	-82.73	-87.81	-73.86
α_{yy}	-70.76	-92.01	-93.64	-85.13
α_{zz}	-71.35	-99.63	-105.33	-91.38
α_0	-76.70	-91.46	-95.59	-83.46
$\alpha(esu) * 10^{-24}$	-11.37	-13.55	-14.17	-12.37
β_{xxx}	0.00	3.00	26.22	-13.72
β_{xyy}	0.00	16.86	3.93	17.15
β_{xzz}	0.00	-3.38	16.47	-6.69
β_x	0.00	16.48	46.62	-3.26
β_{yyy}	0.00	53.18	-64.00	-34.45
β_{xyx}	0.00	3.46	-30.20	4.96
β_{yzz}	0.00	-11.73	-53.29	16.86
β_y	0.00	44.91	-147.50	-12.63
β_{zzz}	0.00	0.00	0.00	0.00
β_{xxz}	0.00	0.00	0.00	0.00
β_{yyz}	0.00	0.00	0.00	0.00
β_z	0.00	0.00	0.00	0.00
$\beta_0(esu) * 10^{-33}$	0.00	47.84	154.69	13.4

into advancements in medicine, considerations for the environment, and the potential of organic electronics. As we draw the curtains on this symphony of insights, we find that halogenation, with its transformative effects, holds the promise of enhancing anthracene's properties across a spectrum of scientific domains, seamlessly blending theoretical understanding with real-world applications.

Contribution of the authors

The authors contributed equally to this article.

Conflict of interests

The authors declare that they have no known competing financial interests or personal relationships that could have influenced the work reported in this paper.

References

1. Rebaz O. Rashid R., Othman K. Exploring The Synthesis of 1,2,4-Triazole Derivatives: A Comprehensive Review. *Journal of Physical Chemistry and Functional Materials*. 2023;6(1): 43–56, <https://doi.org/10.54565/jphcfum.1263834>
2. Omar R. Koparir P., Koparir M. Synthesis of 1,3-thiazole derivatives. *Indian Drugs*. 2021;58(1): 7–19. <https://doi.org/10.53879/id.58.01.12427>
3. Tang M., Yu Q., Wang Z., ... Zhang F. L. Synthesis of polycyclic aromatic hydrocarbons (PAHs) via a transient directing group. *Organic Letters*. 2018;20(23): 7620–7623. <https://doi.org/10.1021/acs.orglett.8b03359>
4. Lawal A. T. and Fantke P. Polycyclic aromatic hydrocarbons. A review. *Cogent Environmental Science*. 2017;3(1): 1339841. <https://doi.org/10.1080/23311843.2017.1339841>
5. Ding Z. B. Tommasini M., Maestri M. A topological model for predicting adsorption energies of polycyclic aromatic hydrocarbons on late-transition metal surfaces. *Reaction Chemistry & Engineering*. 2019;4(2): 410–417. <https://doi.org/10.1039/c8re00229k>
6. Rebaz O. Ahmed L. Koparir P., Jwameer H. Impact of solvent polarity on the molecular properties of dimetridazole. *El-Cezeri Fen ve Mühendislik Dergisi*. 2022;9(2): 740–747. <https://doi.org/10.31202/ecjse.1000757>
7. Mccoull K. D. Rindgen D. Blair I. A. and Penning T. M. Synthesis and characterization of polycyclic aromatic hydrocarbon o-quinone depurinating N7-guanine adducts. *Chemical Research in Toxicology*. 1999;12(3): 237–246, <https://doi.org/10.1021/tx980182z>
8. Sahoo B. M. Ravi Kumar B. V. V., Banik B. K., Borah P. Polyaromatic hydrocarbons (PAHs): structures, synthesis and their biological profile. *Current Organic Synthesis*. 2020;17(8): 625–640. <https://doi.org/10.2174/1570179417666200713182441>
9. Barbosa F., Jr. Rocha B. A., Souza M. C. O., ... Campiglia A. D. Polycyclic aromatic hydrocarbons (PAHs): Updated aspects of their determination, kinetics in the human body, and toxicity. *Journal of Toxicology and Environmental Health, Part B*. 2023;26(1): 28–65. <https://doi.org/10.1080/10937404.2022.2164390>
10. Palmer A. J. Ghani R. A. Kaur N. Phanstiel O., Wallace H. M. A putrescine–anthracene conjugate: a paradigm for selective drug delivery. *Biochemical Journal*. 2009;424(3): 431–438. <https://doi.org/10.1042/BJ20090815>
11. Koparir P., Parlak A. E., Karatepe A., Omar R. A. Elucidation of potential anticancer, antioxidant and antimicrobial properties of some new triazole compounds bearing pyridine-4-yl moiety and cyclobutane ring. *Arabian Journal of Chemistry*. 2022;15(7): 103957. <https://doi.org/10.1016/j.arabj.2022.103957>
12. Haritash A. K., Kaushik C. P. Biodegradation aspects of Polycyclic Aromatic Hydrocarbons (PAHs): A review. *Journal of Hazardous Materials*. 2009;169(1–3): 1–15. <https://doi.org/10.1016/j.jhazmat.2009.03.137>
13. Abdel-Shafy H. I., Mansour M. S. M. A review on polycyclic aromatic hydrocarbons: Source, environmental impact, effect on human health and remediation. *Egyptian Journal of Petroleum*. 2016;25(1): 107–123. <https://doi.org/10.1016/j.ejpe.2015.03.011>
14. Li W., Wu S. Challenges of halogenated polycyclic aromatic hydrocarbons in foods: Occurrence, risk, and formation. *Trends in Food Science & Technology*. 2023;131: 1–13. <https://doi.org/10.1016/j.tifs.2022.11.015>
15. Montgomery Jr. J. A., Frisch M. J., Ochterski J. W., Petersson G. A. A complete basis set model chemistry. VI. Use of density functional geometries and frequencies. *The Journal of Chemical Physics*. 1999;110(6): 2822–2827. <https://doi.org/10.1063/1.477924>
16. Rasul H. H., Mamad D. M., Azeez Y. H., Omer R. A., Omer K. A. Theoretical investigation on corrosion inhibition efficiency of some amino acid compounds. *Computational and Theoretical Chemistry*. 2023;1225: 114177. <https://doi.org/10.1016/j.comptc.2023.114177>
17. Omer R. A. Koparir P., Ahmed L. Theoretical determination of corrosion inhibitor activities of 4-allyl-5-(pyridin-4-yl)-4H-1,2,4-triazole-3-thiothione tautomerism. *Indian Journal of Chemical Technology*. 2022;29(1): 75–81. <https://doi.org/10.56042/ijct.v29i1.51231>
18. Omer R., Koparir P., Koparir M., Rashid R., Ahmed L., Hama J. Synthesis, Characterization and DFT Study of 1-(3-Mesityl-3-methylcyclobutyl)-2-((4-phenyl-5-(thiophen-2-yl)-4H-1,2,4-triazol-3-yl)thio)ethan-1-one. *Protection of Metals and Physical Chemistry of Surfaces*. 2022;58(5): 1077–1089. <https://doi.org/10.1134/S2070205122050185>
19. Costa A. C., Jr. Ondar G. F., Versiane O., ... Tellez Soto C. A. DFT: B3LYP/6-311G (d, p) vibrational analysis of bis-(diethyldithiocarbamate)zinc (II) and natural bond orbitals. *Spectrochimica Acta Part A: Molecular and Biomolecular Spectroscopy*. 2013;105: 251–258. <https://doi.org/10.1016/j.saa.2012.11.097>

20. Tirado-Rives J., Jorgensen W. L. Performance of B3LYP density functional methods for a large set of organic molecules. *Journal of Chemical Theory and Computation*. 2008;4(2): 297–306. <https://doi.org/10.1021/ct700248k>
21. Nasidi I. I., Kaygili O., Majid A., Bulut N., Alkhedher M., ElDin S. M. Halogen doping to control the band gap of ascorbic acid: A theoretical study. *ACS Omega*. 2022; 7(48): 44390–44397. <https://doi.org/10.1021/acsomega.2c06075>
22. Dittmer D. C., Chang P. L., Davis F. A., Iwanami M., Stamos I., Takahashi K. Derivatives of thiacyclobutene (thiete). VI. Synthesis and properties of some thietes. *The Journal of Organic Chemistry*. 1972;37(8): 1111–1115. <https://doi.org/10.1021/jo00973a008>
23. Becke A. D. Density-functional thermochemistry. III. The role of exact exchange. *The Journal of Chemical Physics*. 1993;98(7): 5648–5652. <https://doi.org/10.1063/1.464913>
24. Wilbur D., Manning W. B., Hilton B. D., Muschik G. M. Carbon-13 NMR of polycyclic aromatic compounds. 1-Methoxybenz[a]anthracene-7, 12-diones. *Organic Magnetic Resonance*. 1982;18(2): 63–67. <https://doi.org/10.1002/mrc.1270180202>
25. Aihara J. Reduced HOMO–LUMO gap as an index of kinetic stability for polycyclic aromatic hydrocarbons. *The Journal of Physical Chemistry A*. 1999;103(37): 7487–7495. <https://doi.org/10.1021/jp990092i>
26. Sun Z., Wu J. Open-shell polycyclic aromatic hydrocarbons. *Journal of Materials Chemistry*. 2012;22(10): 4151–4160. <https://doi.org/10.1039/C1JM14786B>
27. Aziz S. B., Abdullah O. G., Hussein A. M., ... Mohammed A. R. Optical properties of pure and doped PVA:PEO based solid polymer blend electrolytes: two methods for band gap study. *Journal of Materials Science: Materials in Electronics*. 2017;28: 7473–7479. <https://doi.org/10.1007/s10854-017-6437-1>
28. Sarmah A., Hobza P. Directly linked metalloporphyrins: a quest for bio-inspired materials. *Materials Advances*. 2020;1(6): 1895–1908. <https://doi.org/10.1039/d0ma00461h>
29. Lazarou Y. G., Prosmittis A. V., Papadimitriou V. C., Papagiannakopoulos P. Theoretical calculation of bond dissociation energies and enthalpies of formation for halogenated molecules. *The Journal of Physical Chemistry A*. 2001;105(27): 6729–6742. <https://doi.org/10.1021/jp010309k>
30. Tang M. L., Bao Z. Halogenated materials as organic semiconductors. *Chemistry of Materials*. 2011;23(3): 446–455. <https://doi.org/10.1021/cm102182x>
31. Akbas E., Othman K. A., Çelikezen F. Ç., ... Mardinoglu A. Synthesis and biological evaluation of novel benzylidene thiazolo pyrimidin-3(5H)-one derivatives. *Polycyclic Aromatic Compounds*. 2023: 1–18. <https://doi.org/10.1080/10406638.2023.2228961>
32. Wang D., Chen L., Shi C., ... Chen Y. Quantum spin Hall insulator in halogenated arsenene films with sizable energy gaps. *Scientific Reports*. 2016;6(1): 28487. <https://doi.org/10.1038/srep28487>
33. Janietz S., Bradley D., Grell M., Giebeler C., Inbasekaran M., Woo E. Electrochemical determination of the ionization potential and electron affinity of poly(9,9-dioctylfluorene). *Applied Physics Letters*. 1998;73(17): 2453–2455. <https://doi.org/10.1063/1.122479>
34. Pearson R. G. Chemical hardness and density functional theory. *Journal of Chemical Sciences*. 2005;117: 369–377. <https://doi.org/10.1007/BF02708340>
35. Chattaraj P. K., Roy D. R. Update 1 of: electrophilicity index. *Chemical Reviews*. 2007;107(9): PR46–PR74. <https://doi.org/10.1021/cr078014b>
36. Mayr H., Patz M. Scales of nucleophilicity and electrophilicity: a system for ordering polar organic and organometallic reactions. *Angewandte Chemie International Edition in English*. 1994;33(9): 938–957. <https://doi.org/10.1002/anie.199409381>
37. Ceylan Ü., Tarı G. Ö., Gökce H., Açar E. Spectroscopic (FT-IR and UV-Vis) and theoretical (HF and DFT) investigation of 2-Ethyl-N-[(5-nitrothiophene-2-yl)methylidene]aniline. *Journal of Molecular Structure*. 2016;1110: 1–10. <https://doi.org/10.1016/j.molstruc.2016.01.019>
38. Esme A. Experimental (FT-IR, FT-Raman, and UV-Vis) and quantum chemical calculations on monomer and dimer structures of 1-hydroxy-2-naphthoic acid using the DFT and TD-DFT methods. *Indian Journal of Pure & Applied Physics (IJPAP)*. 2019;57(11): 822–835. Режим доступа: <http://op.niscpr.res.in/index.php/IJPAP/article/view/21985>
39. Jagdale B. S., Ashok Adole V., Bhavsing Pawar T., Desale B. S. Molecular structure, frontier molecular orbitals, MESP and UV-visible spectroscopy studies of ethyl 4-(3,4-dimethoxyphenyl)-6-methyl-2-oxo-1,2,3,4-tetrahydropyrimidine-5-carboxylate: a theoretical and experimental appraisal. *Material Science Research India*. 2020;17(Special issue 1): 13–26. <https://doi.org/10.13005/msri.17.special-issue1.04>
40. Li A., Draine B. Do the infrared emission features need ultraviolet excitation? The polycyclic aromatic hydrocarbon model in UV-poor reflection nebulae. *The Astrophysical Journal*. 2002;572(1): 232–237. <https://doi.org/10.1086/340285>
41. Arfsten D. P., Schaeffer D. J., Mulveny D. C. The effects of near ultraviolet radiation on the toxic effects of polycyclic aromatic hydrocarbons in animals and plants: a review. *Ecotoxicology and Environmental Safety*. 1996;33(1): 1–24. <https://doi.org/10.1006/eesa.1996.0001>

42. Jones R. N. The ultraviolet absorption spectra of anthracene derivatives. *Chemical Reviews*. 1947;41(2): 353–371. <https://doi.org/10.1021/cr60129a013>
43. Makula P., Pacia M., Macyk W. How to correctly determine the band gap energy of modified semiconductor photocatalysts based on UV-vis spectra. *The Journal of Physical Chemistry Letters*. 2018;9(23): 6814–6817. <https://doi.org/10.1021/acs.jpcllett.8b02892>
44. Wodrich M. D., Corminboeuf C., Schreiner P. R., Fokin A. A., Schleyer P. v. R. How accurate are DFT treatments of organic energies? *Organic Letters*. 2007;9(10): 1851–1854. <https://doi.org/10.1021/ol070354w>
45. Swofford R. L., Long M. E., Albrecht A. C. C–H vibrational states of benzene, naphthalene, and anthracene in the visible region by thermal lensing spectroscopy and the local mode model. *The Journal of Chemical Physics*. 1976;65(1): 179–190. <https://doi.org/10.1063/1.432815>
46. Ricks A. M., Douberly G. E., Duncan M. A. The infrared spectrum of protonated naphthalene and its relevance for the unidentified infrared bands. *The Astrophysical Journal*. 2009;702(1): 301–306. <https://doi.org/10.1088/0004-637X/702/1/301>
47. Szczepanski J., Vala M., Talbi D., Parisel O., Ellinger Y. Electronic and vibrational spectra of matrix isolated anthracene radical cations: Experimental and theoretical aspects. *The Journal of Chemical Physics*. 1993;98(6): 4494–4511. <https://doi.org/10.1063/1.465009>
48. McClellan A. L., Pimentel G. C. Vibrational assignment and thermodynamic properties of naphthalene. *The Journal of Chemical Physics*. 1955;23(2): 245–248. <https://doi.org/10.1063/1.1741948>
49. Srivastava A., Singh V. B. Theoretical and experimental studies of vibrational spectra of naphthalene and its cation. *Indian Journal of Pure & Applied Physics*. 2007;45: 714–720.
50. Haenen H. T. M. Potential probe measurement analysis and charge distribution determination. *Journal of Electrostatics*. 1977;2: 203–222. [https://doi.org/10.1016/0304-3886\(77\)90054-7](https://doi.org/10.1016/0304-3886(77)90054-7)
51. Solano E. A., Mayer P. M. A complete map of the ion chemistry of the naphthalene radical cation? DFT and RRKM modeling of a complex potential energy surface. *The Journal of Chemical Physics*. 2015;143(10). <https://doi.org/10.1063/1.4930000>
52. Pi X., Sun F., Gao J., ... Liu H. A new insight into the SO₂ adsorption behavior of oxidized carbon materials using model adsorbents and DFT calculations. *Physical Chemistry Chemical Physics*. 2019;21(18): 9181–9188. <https://doi.org/10.1039/c8cp07782g>
53. Modelli A., Mussoni L., Fabbri D. Electron affinities of polycyclic aromatic hydrocarbons by means of B3LYP/6-31+G* calculations. *The Journal of Physical Chemistry A*. 2006;110(20): 6482–6486. <https://doi.org/10.1021/jp0605911>
54. Domingo L. R., Aurell M. J., Pérez P., Contreras R. Quantitative characterization of the global electrophilicity power of common diene/dienophile pairs in Diels–Alder reactions. *Tetrahedron*. 2002;58(22): 4417–4423. [https://doi.org/10.1016/s0040-4020\(02\)00410-6](https://doi.org/10.1016/s0040-4020(02)00410-6)
55. Boukabcha N., Benmohammed A., Belhachemi M. H. M., ... Djafri A. Spectral investigation, TD-DFT study, Hirshfeld surface analysis, NCI-RDG, HOMO-LUMO, chemical reactivity and NLO properties of 1-(4-fluorobenzyl)-5-bromolindolin-2,3-dione. *Journal of Molecular Structure*. 2023;1285: 135492. <https://doi.org/10.1016/j.molstruc.2023.135492>
56. Lu T., Chen F. Multiwfn: A multifunctional wavefunction analyzer. *Journal of Computational Chemistry*. 2012;33(5): 580–592. <https://doi.org/10.1002/jcc.22885>
57. Humphrey W., Dalke A., Schulten K. VMD: Visual molecular dynamics. *Journal of Molecular Graphics*. 1996;14(1): 33–38. [https://doi.org/10.1016/0263-7855\(96\)00018-5](https://doi.org/10.1016/0263-7855(96)00018-5)
58. Saidj M., Djafri A., Rahmani R., ... Chouaih A. Molecular structure, experimental and theoretical vibrational spectroscopy, (HOMO-LUMO, NBO) investigation, (RDG, AIM) analysis, (MEP, NLO) study and molecular docking of ethyl-2-[[4-ethyl-5-(quinolin-8-yloxymethyl)-4H-1,2,4-triazol-3-yl] sulfanyl] acetate. *Polycyclic Aromatic Compounds*. 2023;43(3): 2152–2176. <https://doi.org/10.1080/10406638.2022.2039238>
59. Walters W. P., Murcko M. A. Prediction of ‘drug-likeness’. *Advanced Drug Delivery Reviews*. 2002;54(3): 255–271. [https://doi.org/10.1016/s0169-409x\(02\)00003-0](https://doi.org/10.1016/s0169-409x(02)00003-0)
60. Ursu O., Rayan A., Goldblum A., Oprea T. I. Understanding drug-likeness. *WIREs Computational Molecular Science*. 2011;1(5): 760–781. <https://doi.org/10.1002/wcms.52>
61. Ranjith P., Ignatious A., Panicker C. Y., ... Anto P. Synthesis, spectroscopic characterization, DFT, molecular docking and in vitro antibacterial potential of novel quinoline derivatives. *Journal of Molecular Structure*. 2022;1264: 133315. <https://doi.org/10.1016/j.molstruc.2021.131217>
62. Sumathi D., Thanikachalam V., Bharanidharan S., Saleem H., Babu N. R. Vibrational Characterization and Molecular Electronic Investigations of 2-acetyl-5-methylfuran using FT-IR, FT-Raman, UV-VIS, NMR, and DFT Methods. *Journal of Fluorescence*. 2022;32: 1005–1017. <https://doi.org/10.1007/s10895-022-02903-8>

63. Abbas T., Bendjeddou A., Villemin D. Structure, electronic properties, NBO, NLO and chemical reactivity of bis (1, 4-dithiafulvalene) derivatives: functional density theory study. *International Journal of Advanced Chemistry*. 2017;6(1): 18–25. <https://doi.org/10.14419/ijac.v6i1.8668>

64. Villemin D., Abbas T., Bendjeddou A. Molecular structure, HOMO, LUMO, MEP, natural bond orbital analysis of benzo and anthraquinodimethane derivatives. *Pharmaceutical and Biological Evaluations*. 2018;5(2): 27. <https://doi.org/10.26510/2394-0859.pbe.2018.04>

65. Abbas T., Bendjeddou A., Villemin D. Molecular structure, NBO analysis, first hyper polarizability, and homo-lumo studies of π -extended tetrathiafulvalene (EXTTF) derivatives connected to π -nitro phenyl by density functional method. *International Journal of Advanced Chemistry*. 2018;6(1): 114. <https://doi.org/10.14419/ijac.v6i1.11126>

66. Obot I., Macdonald D., Gasem Z. Density functional theory (DFT) as a powerful tool for designing new organic corrosion inhibitors. Part 1: An overview. *Corrosion Science*. 2015;99: 1–30. <https://doi.org/10.1016/j.corsci.2015.01.037>

67. Khan M. U., Khalid M., Asim S., ... Imran M. Exploration of nonlinear optical properties of triphenylamine-dicyanovinylene coexisting donor- π -acceptor architecture by the modification of π -conjugated linker. *Frontiers in Materials*. 2021;8: 719971. <https://doi.org/10.3389/fmats.2021.719971>

68. Al-Shamiri H. A. S., Sakr M. E. M., Abdel-Latif S. A., ... Elwahy A. H. M. Experimental and theoretical studies of linear and non-linear optical properties of novel fused-triazine derivatives for advanced technological applications. *Scientific Reports*. 2022;12(1): 19937. <https://doi.org/10.1038/s41598-022-22311-z>

Information about the authors

Yousif Hussein Azeez, MSc in Advanced Materials Science, Lecturer at the Department of physics, Halabja University (Iraq).

<https://orcid.org/0000-0001-5357-7856>

yousif.husain@uoh.edu.iq

Khdir Ahmed Othman, MSc In Organic Chemistry, Lecturer at the Department of Chemistry, Faculty of Science and Health, Koya University, (Kurdistan Region – F.R., Iraq).

<https://orcid.org/0000-0002-7763-2976>

khdir.ahmed@koyauniversity.org

Rebaz Anwar Omer, PhD in Organic Chemistry, Head of Chemistry Department, Faculty of Science and Health, Koya University (Kurdistan Region – F.R., Iraq).

<https://orcid.org/0000-0002-3774-6071>

rebaz.anwar@koyauniversity.org

Rebaz Obaid Kareem, MSc in General Physics, Lecturer at the Department of Physics, Faculty of Science/ Physics Department, Halabja University (Kurdistan Region – Iraq).

<https://orcid.org/0000-0001-6273-1309>

rebaz.kareem@uoh.edu.iq

Received 16.12.2023; approved after reviewing 14.03.2024; accepted for publication 15.03.2024; published online 25.06.2024.